Development of a Portable COTS-Based CW Radar System at 2.4 GHz

Gogoi, Pallab Kr; Mandal, Mrinal Kanti; Li, Changzhi

DOI
10.1109/MMM.2025.3539244

Publication date
2025

Document Version
Final published version

Published in
IEEE Microwave Magazine

Development of a Portable COTS-Based CW Radar System at 2.4 GHz

Pallab Kr Gogoi, Mrinal Kanti Mandal, and Changzhi Li

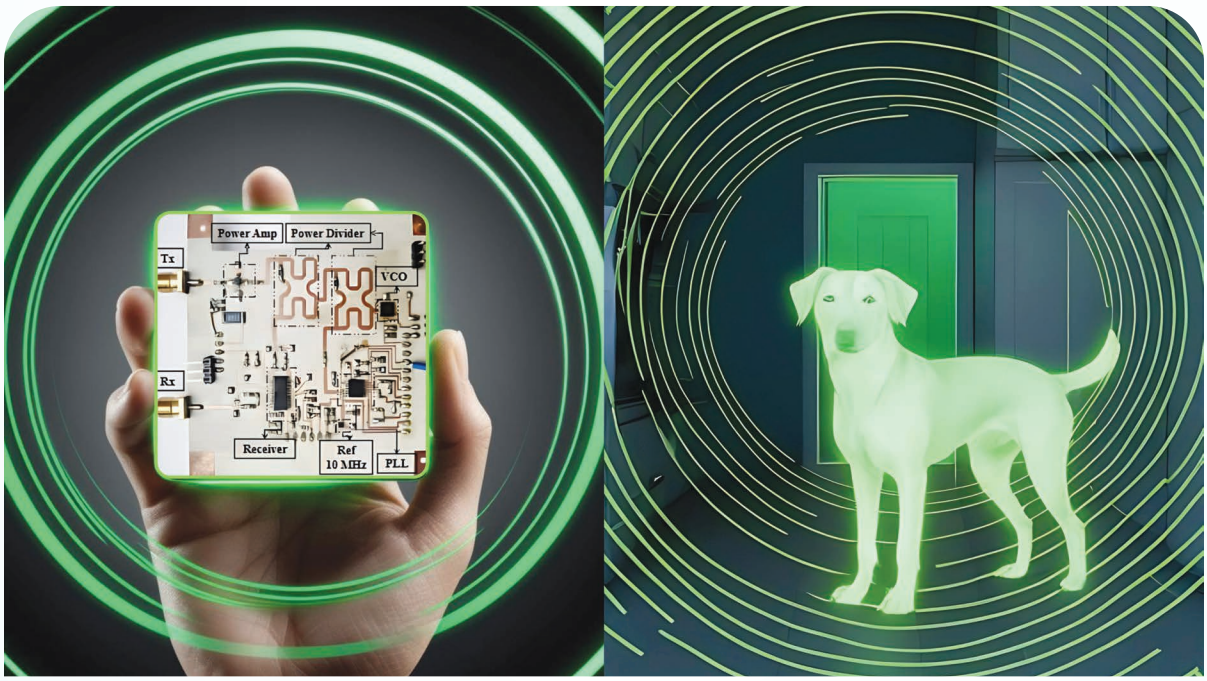

Pallab Kr Gogoi (pkgogoi@ieee.org) is with the Faculty of Aerospace Engineering, Delft University of Technology, 2629 HS Delft The Netherlands. Mrinal Kanti Mandal (mkmandal@ece.iitkgp.ac.in) is with the Department of Electronics and Electrical Communication Engineering, Indian Institute of Technology, Kharagpur 721302, West Bengal, India. Changzhi Li (Changzhi.Li@ttu.edu) is with the Department of Electrical & Computer Engineering, Texas Tech University, Lubbock, TX 79409–3102 USA.

Digital Object Identifier 10.1109/MMM.2025.3539244
Date of current version: 8 October 2025

Over the years, noninvasive contactless sensing has gained popularity due to the availability of numerous commercial off-the-shelf components (COTS). Initially used primarily for military and defense purposes, radar technology has expanded its applications into various civilian sectors where it holds significant potential for aiding humanity directly.

Introduction

A brief history of radar evolution, highlighting key milestones such as the introduction of the resonant cavity magnetron, was reported by Sarkar et al. [1]. This evolution spans from the early 20th century through World War II to the development of modern radar systems, demonstrating significant advancements in both technology and applications across various frequency bands. Additionally, Kalkan [2] provided a comprehensive overview of radar types, including their different categories, applications, and frequency bands.

However, in recent years, the use of short-range portable microwave radars has gained significant attention due to their potential to enhance service quality across various fields, including health care, agriculture, infrastructure maintenance, and security applications [3], [4], [5], [6], [7], [8]. One of the earliest documented uses of radar technology in physiological monitoring dates back to 1975, when an X-band radar was employed to measure the breathing signals of both a rabbit and a human subject [9].

The time-frequency analysis of baseband signals extends beyond motion detection, offering a dynamic method for short-range radars to interpret motion patterns. This capability has led to diverse applications, including gait analysis, fall detection, gesture characterization, and occupancy detection in both military and civilian contexts [10], [11]. With the advancements in radar signal processing and artificial intelligence (AI) algorithms, radars have found extensive use in contactless vital signs detection, human activity classification, and security surveillance applications [12], [13], [14].

In health care, radar modules can be particularly advantageous for monitoring the sleep apnea of individuals, especially the elderly and those with conditions like Alzheimer's and Parkinson's, who require continuous yet privacy-preserving care [15]. Traditional hospital setups for round-the-clock monitoring are impractical and strain health-care facilities and personnel. Radars can even detect semicardiograms, which capture heart contraction and blood ejection patterns [16]. By analyzing these combined with vital signs and camera-based data, radars can enable the contactless monitoring of a person's mental health [17].

Similarly, industrial applications benefit significantly from time-frequency analysis of short-range radar signals. This technology offers an excellent opportunity to monitor the status of rotating structures like windmills in real time [18]. Intelligent microwave radar sensors for structural condition monitoring can address global aging infrastructure issues by capturing the mechanical vibrations and deflections of building structures [19].

Alternative technologies like light-based cameras, sound-based ultrasonic sensors, piezoelectric vibration monitors, and wearables each have limitations. Cameras are cost-effective but raise privacy concerns and need ambient light. Ultrasonic sensors are precise for stationary targets but are affected by noise and temperature. Piezoelectric systems require contact with structures and can wear out. Wearables are accurate but can be uncomfortable and prone to damage.

Regardless of the specific application, integrating radar technology into daily life represents a new frontier for innovation. As radar technology becomes increasingly relevant in various fields, students and professionals have access to a wealth of online resources to enhance their understanding. Free massive open online courses from platforms like the National Program on Technology Enhanced Learning (NPTEL) and Massachusetts Institute of Technology (MIT) OpenCourseWare offer valuable courses on radar systems, covering essential principles and fundamental concepts [20], [21].

Bridging this gap through dedicated projects and specialized workshops can significantly enhance learning by providing practical experience alongside theoretical study. Similarly, engineering design competitions [22], such as the Radar Student Design Competition at the IEEE International Microwave Symposium (IMS) organized by the IEEE Microwave Theory and Technology Society (MTT-S), have been bridging the gap between theory and practice by motivating students to tackle real-world problems since 2014. Winning teams are also invited to publish their innovative solutions in *IEEE Microwave Magazine* [23], [24]. A collage of some of the pictures taken during the maiden IMS design competition held in Tampa, FL, USA, in 2014 is shown in Figure 1.

Moreover, radars created as a part of class projects can evolve into significant research contributions. The low-cost novel two-port transceiver chain that was developed by students in the ECE 5349 "Modern Radar Circuits and Systems" course at Texas Tech University for small motion detection and human range tracking and then progressed from a class assignment to a published research article is an excellent example [25]. Such projects highlight how work undertaken in both competitive and academic settings can lead to advanced

research and real-world applications, demonstrating the broader impact of hands-on learning experiences in engineering education.

In recent years, advanced radar systems have been developed and reported on various venues. For example, Dwyer and Ricketts [26] designed a hand-fabricated frequency-modulated continuous-wave (FMCW) radar to teach radar fundamentals, but it lacks portability and plug-and-play functionality [26]. Similarly, a sophisticated 100 Gbit/s digital millimeter-wave multiple-input, multiple-output radar system described in an "Application Notes" column uses a Xilinx RFSoC and eight transceiver monolithic microwave integrated circuits (ICs), posing challenges for educational environments with limited resources [27]. These examples highlight the need for more adaptable and resource-friendly radar systems in curricula. MIT also guides students in creating small radar systems for range, Doppler, and synthetic aperture radar imaging [28]. Additionally, most commercial radars at 24 or 77 GHz, used mainly in automotive applications, cannot be built from scratch by students in class, limiting students' understanding of design constraints.

In educational settings, especially when teaching complex systems like radar, there is a pressing need to simplify both the design and implementation processes to make them more accessible to students, thereby bridging the digital divide in underdeveloped and developing nations [29]. While the existing literature often delves into specific aspects, such as chip design and application-specific details, and frequently focuses on commercially available radars and discrete lab equipment and components, it often overlooks the design of a portable and compact radar module using COTS-based components and in-house fabrication facilities for conducting educational as well as research-based experimentation.

Such limitations are particularly evident in environments that emphasize entrepreneurial mindsets and self-directed learning. For instance, in project-based embedded systems design courses [30], entrepreneurial thinking [31] can significantly enhance students' ability to frame design problems and support self-directed learning. By focusing on modular simplified radar designs, educators can address these challenges, providing students with a comprehensive understanding of radar systems while fostering innovative problem-solving skills applicable to real-life situations.

Providing a comprehensive perspective on modern radar system development, this work adopts a more integrated approach.

This article addresses these issues by enabling students to design radar systems from the ground up, highlighting the importance of each component, from RF to baseband. Unlike existing tutorials that focus on SubMiniature version A-based module connections, this work advances the field by miniaturizing radar systems and transitioning from modular to integrated printed circuit board (PCB)-level designs. This shift reduces the size of radar systems and enhances their functionality and application potential, reflecting progress in radar technology and design while offering substantial educational benefits.

Figure 1. *(a)–(d) IEEE MTT-S IMS High-Sensitivity Radar Student Design Competition Winners in 2014.*

Providing a comprehensive perspective on modern radar system development, this work adopts a more integrated approach, creating additional learning opportunities and embracing a systems engineering perspective in designing a portable radar [32]. It discusses critical aspects necessary for building and prototyping a plug-and-play 2.4-GHz Doppler radar, serving as a generalized framework that addresses various design considerations and offers a detailed guide for students and practitioners. This article is an extended version of a conference paper [33], elaborating on the complete design procedure, including theoretical aspects, in a tutorial format.

The article is structured as follows. It begins with a tutorial explanation of radar fundamentals, followed by a systematic overview of radar architecture and the design of its various blocks. Finally, experiments are conducted to validate the design.

Fundamentals

As an acronym for "radio detection and ranging," radar uses radio waves to determine the distance (ranging), direction, and velocity of objects relative to the system. A basic radar system comprises a transmitter (Tx) and a receiver (Rx) separated by a distance, R_B, as shown in Figure 2. The Tx emits electromagnetic waves with power, P_T, which reflect off objects located at a distance R_1. The Rx, positioned at a distance R_2 from the object, collects these reflections to determine the presence and location of targets. The target's detectability is quantified by its radar cross-section, σ. When $R_B = 0$, the system is known as a *monostatic radar*, and in this case, $R_1 \sim R_2 = R_{\max}$ [34].

However, if $R_B \neq 0$, the system is known as a *bistatic radar*, and in this case, R_1 may not be equal to R_2. Most commercially available radars used in civilian applications are monostatic in nature. Radars can be broadly classified based on either the waveforms emitted or the architecture. Based on the waveform, they be categorized into *single-tone CW* or *pulsed-wave* radars. Further, the transmitted frequency can be either a *single-tone CW radar* that transmits continuously with a fixed amplitude and frequency or an *FMCW radar* that includes frequency modulation in its transmitted signal.

CW radar has the advantage of simple design and can effectively measure the relative velocity of a target through the Doppler effect. However, it cannot determine the range of the target and is susceptible to interference from other sources. FMCW radar, on the other hand, can measure both the range and velocity of a target due to its frequency modulation. It offers range resolution to differentiate targets based on their distances but is more complex and costly to implement. Pulsed radar, which transmits in short bursts, is also capable of measuring the range of a target directly. However, it requires more sophisticated timing and synchronization systems, making it more complex and expensive to build and maintain compared to CW radar.

Rx architectures, on the other hand, can be either *homodyne* or *heterodyne*. In the homodyne architecture, the received signal is multiplied by a local oscillator (LO) of the same frequency as the transmitted signal, making it simpler and commonly implemented with a single mixer or quadrature mixer. However, it faces challenges such as dc

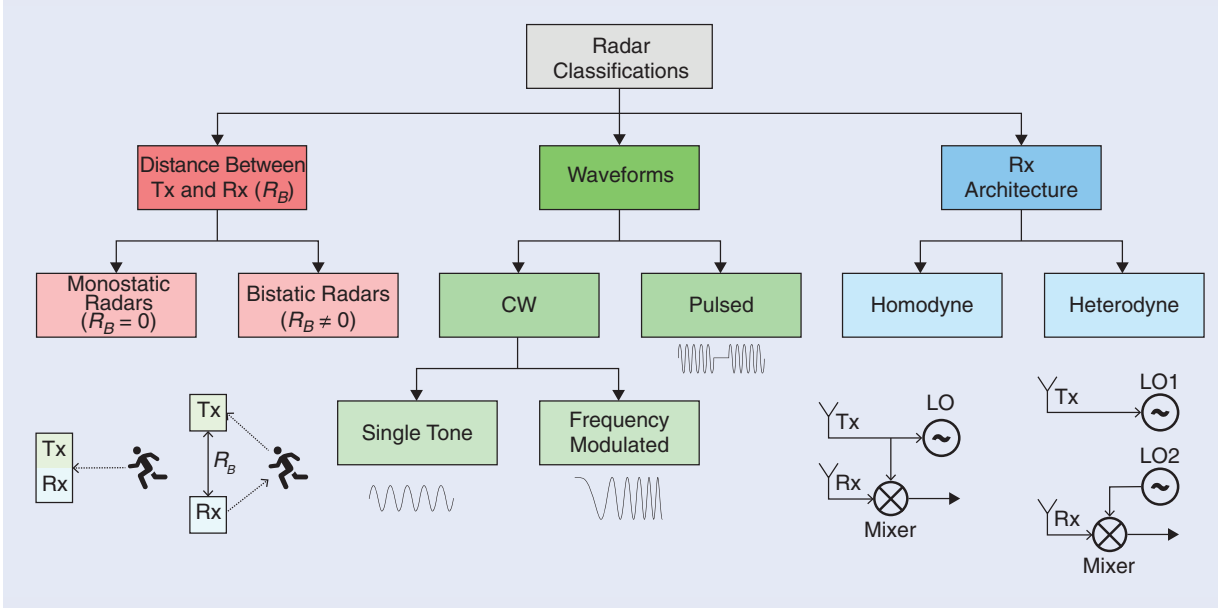

Figure 2. *Various classifications of radars. CW: continuous wave; Tx: transmitter, Rx: receiver.*

offsets, in-phase and quadrature (I/Q) imbalance at RFs, and nonlinearity. In contrast, the *heterodyne* architecture uses a different LO frequency to create an intermediate frequency (IF) before final processing. This approach can improve performance by mitigating some of the homodyne issues but requires more complex hardware. The classification of radar systems used in this work is summarized in Figure 2, highlighting the different categories.

In this article, the design and theoretical aspects of a portable CW radar with homodyne architecture are considered. The inbuilt radar module can be modified according to user requirements, allowing for the design of custom radar modules for specific experiments with minimal modifications to the original module, making it suitable for educational as well as research purposes.

CW Radar for One-Way Motion Detection

Let us consider a CW wave with angular frequency, $\omega_o = 2\pi f_o$. Let r_0 be the initial distance of the target and v_r be the radial velocity of the target, as shown in Figure 2. The transmitted signal is given by $S(t) = A_t \sin(\omega_o t + \phi)$. Since the target is moving, $r(t) = r_0 \mp v_r(t - t_0)$. Thus the received signal can be simplified as the following:

$$R(t) = A_r \sin\left[(\omega_o \pm \omega_d)t - \frac{2\omega_o r_o}{c} \mp \omega_d t_o + \phi\right]. \tag{1}$$

Here, the negative sign indicates an approaching target, and the positive sign indicates a receding target. After mixing with the transmitted signal along with low-pass filtering and amplification, the Doppler frequency $f_d = 2f_o v_r / c$ can be recovered, which allows us to interpret the velocity of the target. After mixing, the sign of the Doppler frequency is lost; thus, a quadrature mixture is usually preferred over the simple mixer, indicating whether the target is receding or approaching.

CW Radar for Reciprocal Motion Detection

Figure 3 illustrates a vibrating source undergoing uniform oscillations $x(t)$ at a distance d_o from the radar. According to established Doppler theory, a target with time-varying displacement produces a phase-modulated signal proportional to its position [35]. In this context, the CW radar is used for reciprocal motion detection (RMD). Here, the term "vibrating" denotes that the target is exhibiting reciprocal motion, implying an oscillatory or periodic movement. As a result, the phase modulation induced by the target's displacement allows the radar to detect and analyze this reciprocal motion through variations in the received signal.

In this article, the design and theoretical aspects of a portable CW radar with homodyne architecture are considered.

The radar transmits a single-tone signal $T(t) = a_0 \cos(2\pi f_o t + \phi_1(t))$, where a_0 is the amplitude, f_o represents the frequency of oscillation of the LO, and $\phi_1(t)$ denotes the phase noise introduced by the LO. After illumination of the target by $T(t)$, which is vibrating with a displacement of $x(t)$, the received signal in the CW radar for RMD is given by the following:

$$R(t) = b_0 \cos(2\pi f_o(t - d(t)) + \phi_2(t)) \tag{2}$$

where $\phi_2(t)$ is the phase noise after the signal is reflected back from the object with $d(t)$ given by the following:

$$d(t) = \frac{2d_0}{c} + \frac{2x(t)}{c} \tag{3}$$

$$I(t) = A_0 + c_0 \cos\left[\frac{4\pi x(t)}{\lambda} + \phi(t)\right] \tag{4}$$

$$\phi(t) = \frac{4\pi d_0}{\lambda} + \phi_1(t) - \phi_2(t). \tag{5}$$

Equation (4) is obtained after mixing and applying a low-pass filter. Here, b_0 and c_0 are constants, and A_0 is the dc offset due to the homodyne architecture.

Range correlation theory states that $\phi_1(t) - \phi_2(t)$ can be considered to be a constant as the homodyne architecture ensures coherent demodulation, and the distance between the object and the CW radar for RMD is not far apart [36], [37]. Hence, (5) simplifies to the following:

$$I(t) = A_0 + c_0 \cos\left[\frac{4\pi x(t)}{\lambda} + \theta\right]. \tag{6}$$

Using the small signal approximation and given that $x(t)$ is small compared to the wavelength of operation of the CW radar for RMD, the following conditions can be deduced:

1) The optimum point occurs when the system provides the best performance with a minimum

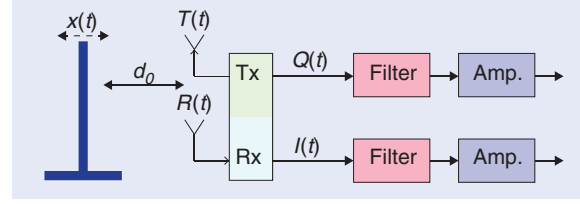

Figure 3. *An illustration showing a vibrating object placed at a fixed distance d_0 from the CW radar. Amp.: amplifier.*

signal-to-noise ratio (SNR) and the output becomes a linear function of the vibration of the target. Since a cosine signal was considered initially, the optimum point occurs when the argument of the cosine function is an odd multiple of $\pi/2$. The resulting output signal is given by the following:

$$I(t) = A_0 + c_{00}\frac{4\pi x(t)}{\lambda}. \tag{7}$$

2) Null points occur when the argument of the cosine function is an even multiple of $\pi/2$, resulting in the output signal given by the following:

$$I(t) = A_0 + c_{01}\left[1 - \left\{\frac{4\pi x(t)}{\lambda}\right\}^2\right]. \tag{8}$$

Thus, sensitivity is degraded since the output signal is no longer linearly proportional to the time-varying displacement. Here, c_{00} and c_{01} are constants.

The problem of null points [38] is mitigated by the use of a quadrature demodulator, which generates the quadrature-phase component of the signal simultaneously, given by the following:

$$Q(t) = B_0 + c_o \sin\left[\frac{4\pi x(t)}{\lambda} + \theta\right]. \tag{9}$$

Here, B_0 is the dc offset in the quadrature-phase component. Since the signal is 90° out of phase with the previously analyzed signal, whenever (7) goes to a null point, (9) reaches the optimum point due to its quadrature nature, thus maintaining detection linearity and maximum signal sensitivity for the RMD across its range.

To resolve the uncertainty of which channel contains a better signal, advanced methods, such as arctangent demodulation, complex signal demodulation, and extended differentiate and cross-multiply algorithms, have been used to combine I/Q components for robust measurement that is immune from the null-detection point problem [39], [40], [41]. Additionally, dc offsets due to the homodyne architecture pose a significant challenge as micro-Doppler signals are often buried within the dc signal [42]. Furthermore, mismatches in the dc offsets for the I and Q components' amplitude and phase response can complicate the compensation process [43]. Without advanced signal processing algorithms, it can be challenging for students to test their radar kits effectively and observe signals clearly on an oscilloscope.

This situation underscores the importance of a systems-level perspective in radar design. By incorporating simple corrective measures to the baseband signal, it is possible to develop handheld radar systems that are accessible to students and hobbyists. Such systems can facilitate a deeper understanding of radar principles and design. The next section of this article addresses this issue.

Radar Architecture

For design simplification, the portable radar architecture in this article is divided into four key units arranged in chronological order as follows:

1) *RF unit:* This unit comprises the Tx and Rx blocks responsible for transmitting and receiving the radar signals, along with the signal conditioning and enhancing parts.
2) *Baseband unit:* This unit contains all the low-frequency circuitry required to control the radar and processes the received signals to extract the relevant information.
3) *Power unit:* This unit provides the necessary dc power to all the other units in the radar system.
4) *Control and acquisition unit:* This unit manages the overall control of the radar system and acquires data for further analysis using a microcontroller.

Each unit of a portable radar system plays a distinct role, and the system can be constructed using a top-down approach, beginning with the RF unit and ending with the power unit. The generalized block diagram for the proposed radar module is shown in Figure 4. The main advantage of this approach is that, although each unit is interconnected, it allows for modifications to specific parts of the design without affecting the other units. This modularity ensures that changes or improvements can be made more efficiently and with greater flexibility.

RF Unit

The RF unit can be further subcategorized into three main blocks: the Tx, the Rx, and signal distribution and enhancement (SDE). The Tx generates the RF signals, incorporating the RF oscillator. The Rx captures incoming RF signals, converting them into baseband signals through components such as mixers. The SDE facilitates the distribution of RF signals between the Tx and Rx, including power dividers and power amplifiers (PAs), gain blocks, and filters to manage signal strength, integrity, and purity.

Tx

The core of the proposed radar module is a voltage-controlled oscillator (VCO). However, in many cases, VCOs are not inherently stable, and the selection of the Tx frequency must be accurate to the kilohertz level. Moreover, when using the Industry, Science, Medicine (ISM) band, it is crucial to ensure that the transmitted frequency is within the required bandwidth (BW) to avoid interference with other systems. Thus, in this work, the Tx unit involves a VCO-phase-locked loop

(PLL) system to ensure precise frequency stability and prevent interference, thereby enhancing the overall performance of the radar.

The availability of COTS-based PLLs provides an additional advantage, allowing for frequency control accurate to kilohertz levels using a simple serial peripheral interface (SPI) that can be implemented on an Arduino, which is one of the most popular and user-friendly microcontrollers without the need for extensive embedded C programming knowledge. However, based on application-specific needs and the requirement for higher resolution analog-to-digital converters (ADCs) or better microcontrollers like the Raspberry Pi Pico, they can be easily integrated within the designed radar module with minimal changes, ensuring its modularity and adaptability for various precision demands.

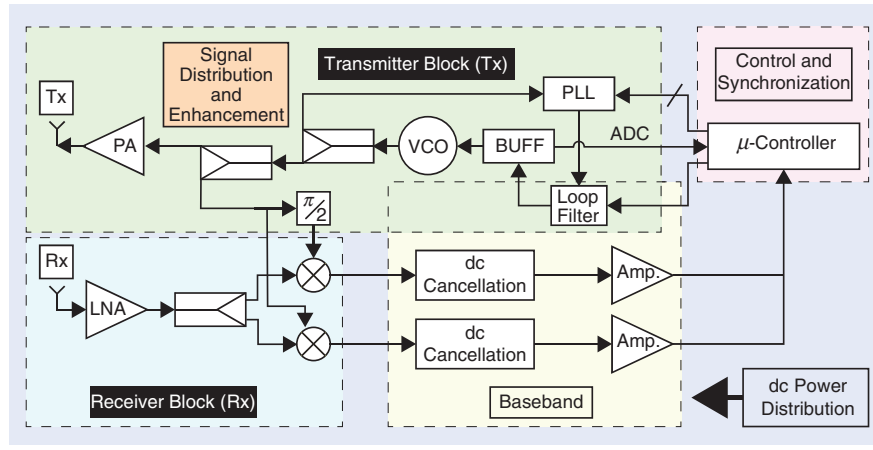

Figure 4. *A block diagram of the proposed radar module. PA: power amplifier; VCO: voltage-controlled oscillator; LNA: low-noise amplifier; PLL: phase-locked loop; BUFF: buffer.*

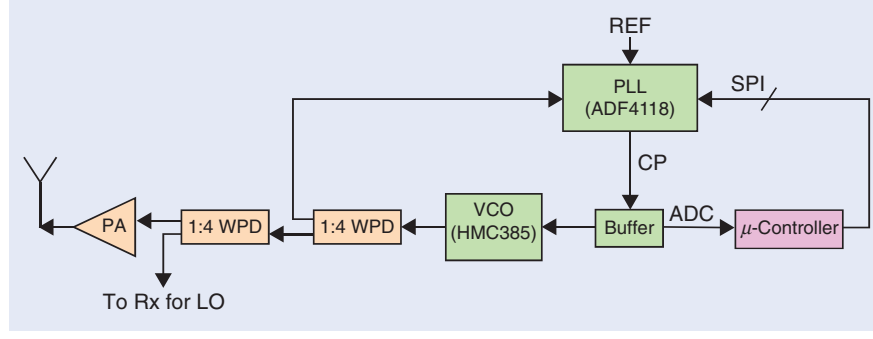

Figure 5. *A block diagram of the Tx. WPD: Wilkinson power divider; CP: charge pump; REF: reference.*

The block diagram of the Tx is shown in Figure 5. Standard 50-Ω microstrip lines are employed for routing the RF signal, with all RF chips contained on a single layer to avoid any loss due to discontinuity. The ICs used are compact, minimal cost, and easy to interface with any microcontroller.

For this work, HMC385 is used as the VCO. It is capable of generating frequencies from 2.25 to 2.5 GHz with a maximum power level of 4.5 dBm with a tuning range from 0 to 10 V [44]. The RF output is provided through pin 16 of the chip, which is single ended. Similarly, ADF4118 is the PLL chip used in this work, which has a maximum frequency range of 3 GHz [45]. The RF signal is sampled using a power divider, with the output fed to pin 6 via a single-ended line. Pin 5 is ac coupled to the ground using a capacitor of 10 pF. Pins 11, 12, and 13 are used for SPI communication, while pin 10 is the chip enable pin, which can be set high or low to enable or disable the PLL. Pin 2 is the charge pump (CP) output, which connects through the loop filter to pin 22 of the VCO, completing the loop.

The biasing of the ICs was accomplished according to the datasheet requirements, and unused pins were left open circuited. To provide the stable clock required for PLL operation, a MEMS-based oscillator, the DSC6003HI3B, is connected to pin 8 of the PLL IC [46].

Rx

A crucial component in an Rx block is the quadrature mixer for down-converting the received RF signal into two orthogonal signals, known as the *I and Q components*. Several standard chips are available commercially, but to make the radar module versatile and miniature, a communication Rx IC, the AD8347, was

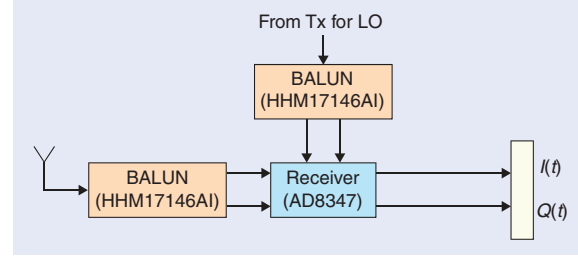

Figure 6. *A block diagram of the receiver. BALUN: balanced to unbalanced.*

used. This IC can be used for an RF range between 800 MHz and 2.7 GHz [47]. The LO signal required for mixing is sampled from the Tx block, as shown in Figure 6. This IC includes an inherent low-noise amplifier (LNA) with controllable gain.

Although the IC provides various functionalities for processing baseband signals directly, for simplicity, the I/Q signals are directly sampled from pin 8 and pin 22, which are single ended. The RF signals used for LO mixing and the received RF signals are differential in nature. Pin 1 and pin 28 are used for the LO input, with the LO drive set at −8 dBm. Pins 10 and 11 are designated for the received RF signals. The IC has a maximum noise figure (NF) of 11 dB. The IC is biased as per the datasheet specifications, and any unused pins are left unconnected.

SDE

To sample the required power for the VCO-PLL loop and the LO signal in the Rx IC at the appropriate power levels and BWs, RF power dividers are needed. However, conventional power dividers for unequal splits are typically constrained by the need for quarter-wavelength transformers and high-impedance line requirements, which can lead to issues with size and implementation.

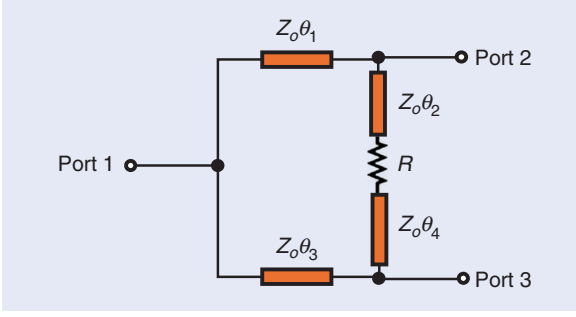

Figure 7. *A schematic of the power divider with an unequal dividing ratio ($Z_0 = R = 50\ \Omega$)*

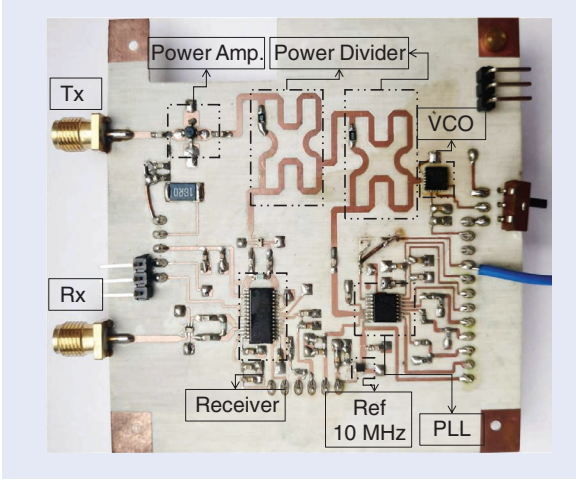

Figure 8. *A photograph of the fabricated RF unit (size: 70 mm × 70 mm substrate: 0.813 mm RO4003C, $\epsilon_r = 3.55$).*

Moreover, the use of lumped components can introduce additional losses due to their lower quality, and most COTS-based chips do not provide that option for unequal power division. To address these issues, an unequal power divider utilizing only 50-Ω characteristic impedance is implemented in this work [48].

Figure 7 illustrates the schematic of the power divider, where Z_0 represents the characteristic impedance of the microstrip line, θ denotes the electrical length, and R is the isolation resistor. The power dividing ratio is described as $k_2 = P_2/P_1$ (with $k_2 > 0$). Additionally, the parameter x is defined by the following:

$$x = \sqrt{\frac{2\left(k^2 + 1 - \sqrt{k^4 - k^2 + 1}\right)}{3}}. \tag{10}$$

The electrical lengths are then given by the following equations:

$$\theta_1 = \cot^{-1}\left(\frac{\sin\theta_2 \sin\theta_4 - k}{\sin(\theta_2 + \theta_4)}\right) \tag{11}$$

$$\theta_2 = \cos^{-1}(x) \tag{12}$$

$$\theta_3 = \sin^{-1}(k \sin\theta_1) \tag{13}$$

$$\theta_4 = \cos^{-1}\left(\frac{x}{k}\right). \tag{14}$$

If the results from the equations are negative, an additional length of 360° must be added to the result. For example, for a power dividing ratio of 1:4, the respective values using the equations give $\theta_1 = 151.2°$, $\theta_2 = 14.85°$, $\theta_3 = 106.21°$, and $\theta_4 = 59.95°$. A relative BW of 15% is usually achievable for this design, which is sufficient for the present application.

To compensate for power loss during distribution, a COTS-based PA, AG302-86 [49], is incorporated to enhance the Tx output. Given the nonlinear nature of amplifiers, an additional bandpass filter may be required depending on the specific application. Both components can be tailored to suit the target application. Since the selected Rx IC already included an on-chip LNA, the use of an additional one was not necessary in this case.

Finally, the use of balanced-to-unbalanced (BALUN) lines is essential when using differential Rx and Tx chips. For this work, the compact surface-mount device (SMD) BALUN HHM17146A1 is used [50].

The need to designate this unit as a separate SDE unit arises from its role in providing flexibility and adaptability within the radar's RF module. The need to designate this unit as a separate SDE unit arises

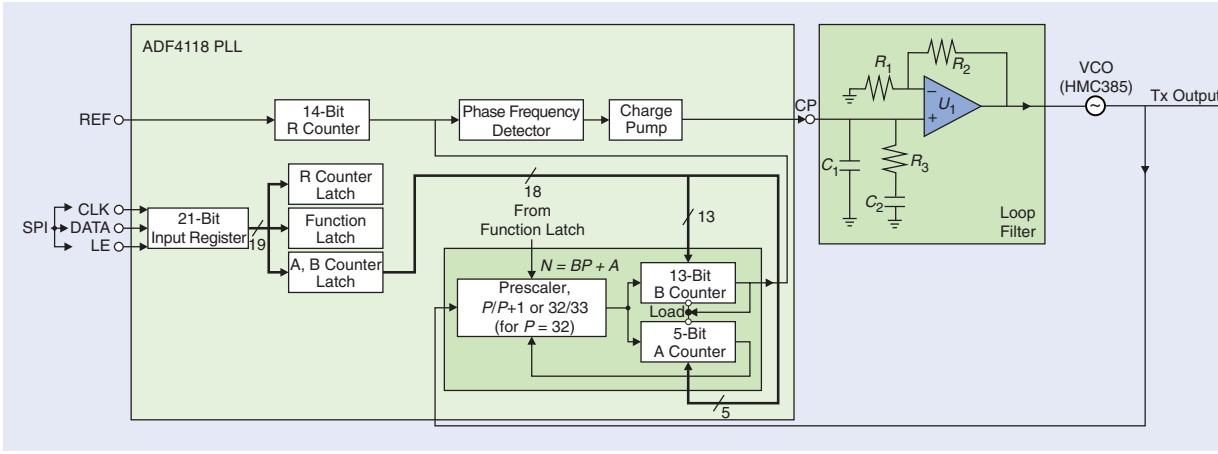

Figure 9. *A block diagram of the complete ADF4118 PLL-VCO loop ($R_1 = R_2 = 1$ kΩ, $R_3 = 18$ kΩ, $C_1 = 22$ μF, and $C_2 = 10$ nF). CLK: clock; LE: latch enable.*

from its role in providing flexibility and adaptability within the radar's RF module. By designating the SDE unit independently from both the Tx and Rx units, it can be tailored to meet specific requirements without affecting the overall circuit configuration and design. This approach allows for modifications and enhancements to the SDE unit while maintaining the integrity of the radar system.

The fabricated unit for the complete RF unit is shown in Figure 8. The total transmitted power from this board is around 10 dBm. The sensitivity of the Rx, with an NF of 11 dB, operating over a BW of 1 MHz and requiring an SNR of 10 dB for acceptable performance, is calculated using the following equation. Substituting the given values, the sensitivity of the radar module comes to be –81 dBm.

$$\text{Sensitivity (dBm)} = \text{SNR}_{\text{required}} + \text{NF} + 10\log_{10}(\text{BW}). \tag{15}$$

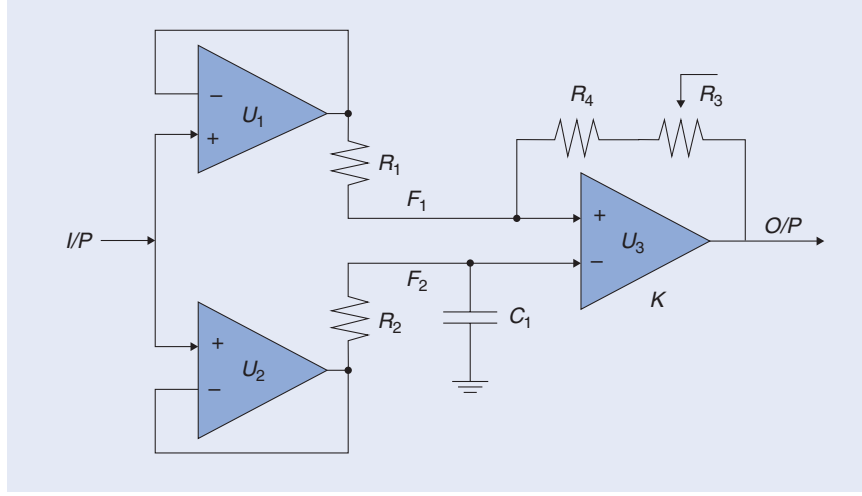

Figure 10. *A schematic of dc cancellation and amplification ($R_1 = R_2 = 1$ kΩ, $R_3 = 10$ kΩ (potentiometer), $R_4 = 1$ kΩ, and $C_1 = 220$ μF).*

Baseband Unit

This is one of the most important parts of the complete radar system. It can be further divided into two parts: the loop filter design and the second baseband amplification and conditioning.

VCO-PLL Loop Design

The loop filter is essential for converting the output current from the charge pump into a voltage suitable for driving the VCO across its entire frequency range. Proper design of the loop filter is critical for achieving a stable VCO-PLL system [51]. It influences the dynamic performance and stability of the PLL, affecting signal quality and frequency accuracy. By carefully selecting filter components, phase noise can be minimized, and lock times can be shortened, thereby enhancing radar system performance.

Since this tutorial focuses on a simplified design approach without delving deeply into the intricacies of PLL design, an easy-to-use open source PLL loop filter design software ADIsimPLL from Analog Devices is utilized [52]. The critical aspect to consider is the tuning range of the VCO, which can be found in the datasheet of the COTS component. If the required tuning voltage exceeds the voltage generated by the charge pump output of the PLL, which is typically less than or equal to the PLL chip's biasing voltage, an active loop filter must be used.

Additionally, to monitor and calibrate the voltage levels without loading the loop filter, a small voltage divider circuit is added through a buffer, which can be directly connected to the ADC of the microcontroller. The use of a voltage divider is optional and depends on the maximum voltage level that the microcontroller can sample. In this case, the Arduino can handle up to 5 V; hence, a voltage divider is used to test the voltage levels. This allows the required VCO tuning graph to be monitored when the control signal is sent to the PLL for generating a particular frequency. The schematic for the loop filter used in this work is shown in Figure 9, but the reader can modify the schematic accordingly as per their requirements.

DC-Offset Compensated Amplifier

Due to the homodyne nature of the architecture, the baseband signal suffers from a significant dc offset, thereby limiting the use of simple amplifiers. Moreover, the micro-doppler (MD) effects are almost near dc, so simply using a capacitively coupled amplifier may not fulfill the purpose. The function of the baseband stage is to amplify and equalize the I/Q signals after mixing to be ready for analog-to-digital conversion. Without this, it is impossible to analyze I/Q data from the radar for object detection.

To address the issue of dc offset in I/Q signals, a simple differential amplifier can be used to subtract the dc offset. However, determining the exact dc values is challenging because they depend on both the Rx IC and various external factors (Figure 10). While the dc offset can be manually tuned using the digital analog converter of a microcontroller to provide a constant dc voltage, this process is often impractical. Therefore, a more efficient method is needed to extract the baseband signal and nullify the offset.

To achieve a robust baseband signal, a copy of the signal with the dc offset, F_1, is made through buffer U1 designed using operational amplifiers (Op-Amps), and one copy is passed through an RC circuit, through buffer U2, as shown in Figure 11. The time constant must be larger than the minimum frequency to be detected. Buffers U1 and U2 are added to provide isolation, ensuring a stable and accurate signal processing environment. Assuming that the signal obtained after down-conversion to baseband is $S(t) + D$, where $S(t)$ is the signal and D is the dc offset, $F_1 = S(t) + D$ and $F_2 = D$. When F_1 and F_2 are passed through a differential amplifier with gain K, the output is $Y(t) = K(F_1 - F_2) = KS(t)$. This Y contains the signal without the dc offset, which can be analyzed by using ADC and signal processing techniques to extract various information. The gain of the circuit is given by the following:

$$K = 1 + \frac{R_3 + R_4}{R_1}. \quad (16)$$

All the Op-Amps used in this work are SMD versions of the LM358 [53]. Resistance R_2 and capacitor C_1 are responsible for generating F_2, which is basically a low-pass filter with a very high

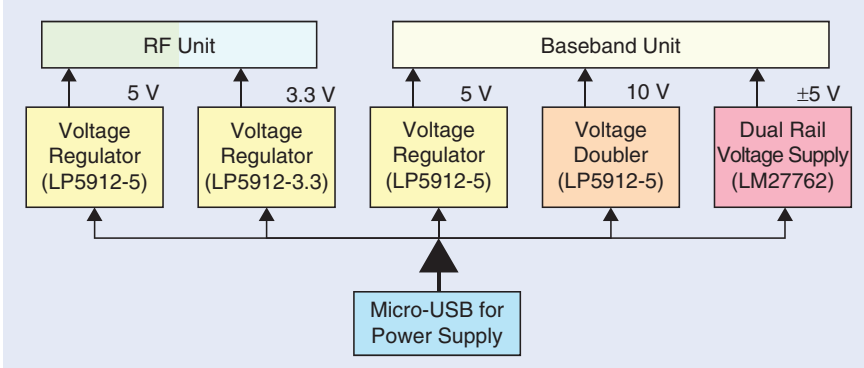

Figure 11. *A block diagram of the power distribution unit with all its ICs named.*

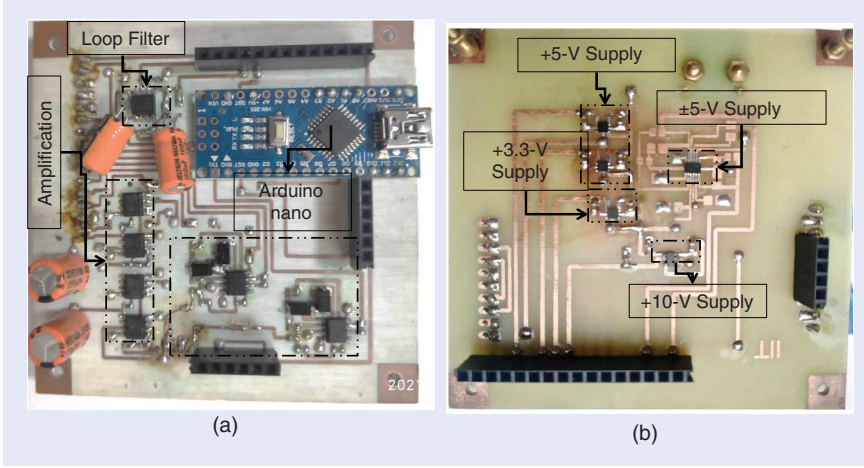

Figure 12. *(a) and (b) Photographs of the fabricated boards (70 mm × 70 mm). (a) Baseband unit, substrate: 0.813-mm RO4003C, $\epsilon_r = 3.55$. (b) Power unit, substrate: 0.5-mm FR4, $\epsilon_r = 3.8$.*

time constant, while R_3 can be a variable resistance to control the baseband gain.

The PCB of the complete baseband unit is designed on the second layer to minimize area usage without causing disturbances to the RF unit. Consequently, if changes are needed, they can be made with minimal alterations to any layer, assuming that the PCB lines are routed according to the first layer. Future designs could potentially replace the current configuration with a single Op-Amp design [54]. The fabricated board is shown in Figure 12(a).

This design approach is useful not only for students and hobbyists but also for researchers who need to rebuild the circuit as needed. This unit also houses the microcontroller. For simplicity, an Arduino Nano is used directly. For further development, any microcontroller chip can be embedded in the design, allowing flexibility for advanced applications and modifications.

Power Unit

The power management module is responsible for providing a constant voltage of a specified value with minimum noise ripple for basing the ICs in RF as well as the baseband modules [55], [56], [57]. A 5-V supply and a 3.3-V supply are used for the RF layer, whereas the rest are used for powering the baseband modules. The block diagram of the power management module is shown in Figure 12.

The USB connection from the laptop is used as the main source of voltage, which can be later replaced with a battery source to make the system portable. The power consumption for the ICs is evaluated across various supply voltages. The measured power consumption is as follows: 707.5065 mW for the 5-V supply, 115.5 mW for the 3.3-V supply, 30 mW for the 10-V supply, and 180 mW for the ±5-V supply. The total power consumption, excluding the additional PA arrangement, is 1033.0065 mW, which approximates to 1 W. Including the PA arrangement, the total power consumption rises to 1.5 W.

To ensure optimal performance and to minimize interference, all RF ICs are biased according to the specifications provided in their datasheets. To further optimize power consumption, each power unit includes an enable pin that can be controlled using the microcontroller to selectively activate or deactivate specific components based on operational requirements. This feature provides flexibility in managing power usage and enhances the overall efficiency of the system.

This design approach is useful not only for students and hobbyists but also for researchers who need to rebuild the circuit as needed.

The final unit incorporates a separate power management layer designed to isolate noise generated by dc-dc conversion from the baseband amplifier. High-value capacitors are employed to further suppress noise, in accordance with datasheet recommendations. The design uses a similar header approach to attach the power management layer to the baseband layer, which in turn connects to the RF layer. This modular approach facilitates easier access and troubleshooting in the event of layer failures during experimentation. The fabricated layout is shown in Figure 12(b).

Control and Data Acquisition

Controlling the ADF4118 PLL IC with a microcontroller is essential. While the ADF4118 evaluation board supports useful modes, such as frequency sweep and frequency hop for FMCW and frequency-shift keying implementations, it requires proprietary software and a constant connection during sweep mode. However, using the evaluation board directly can be a challenge for portability and cost-effectiveness. Since this setup uses only the IC, developing a custom control process is necessary.

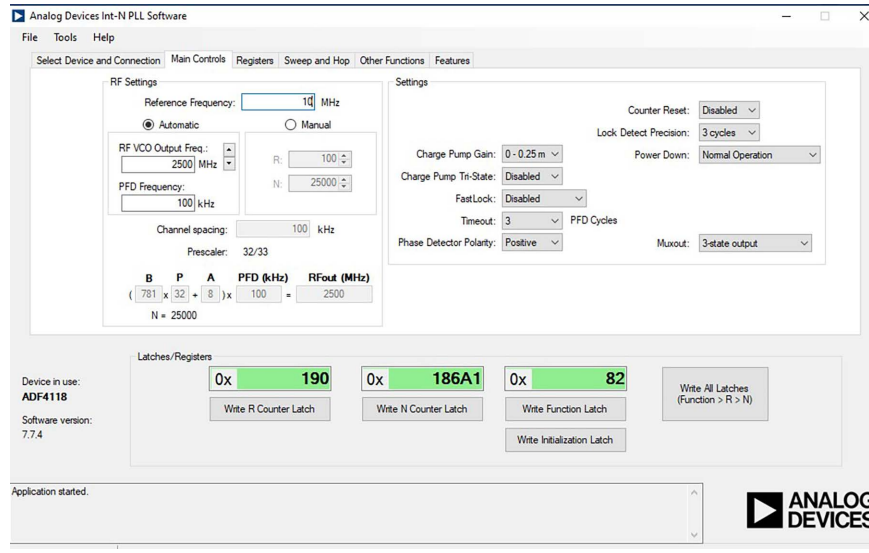

Figure 13. *A screenshot of the software window used for generating the HEX codes.*

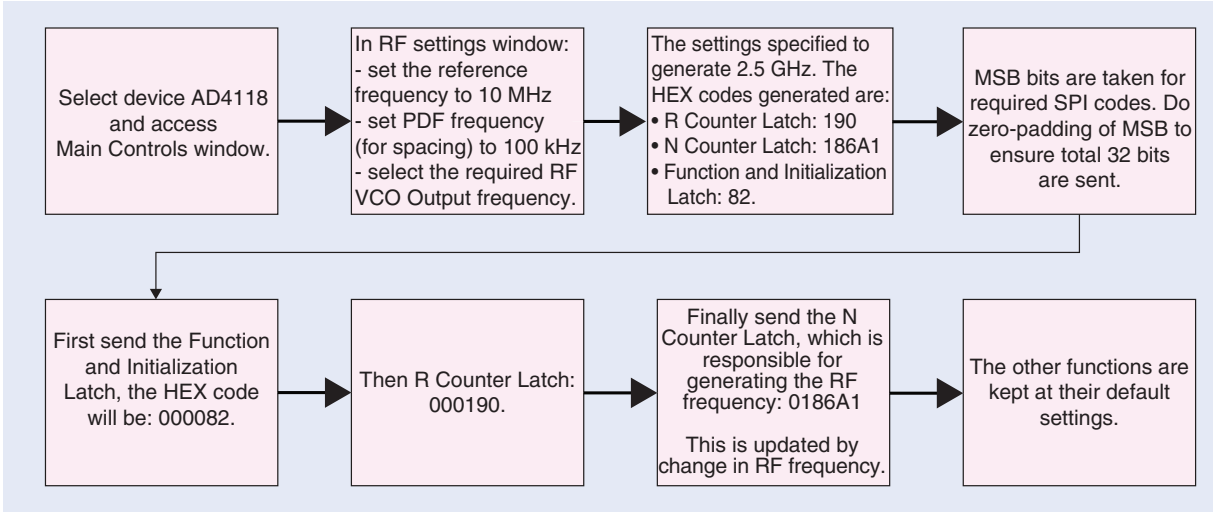

Figure 14. *The workflow for generating an RF frequency of 2.5 GHz using the PLL-VCO loop. PDF: probability density function; MSB: most significant bit.*

The ADF4118 communicates via SPI, with pins 11, 12, and 13 serving as the clock, data, and latch enable pins, respectively. These pins must be accurately connected to the corresponding pins on the microcontroller. According to the datasheet, the N counter latch, R counter latch, and Function/Initialization latch, each 24 bits long, need to be written. This presents a coding challenge as the Arduino Nano, in bootloader mode, can only send 8-bit words via the SPI.

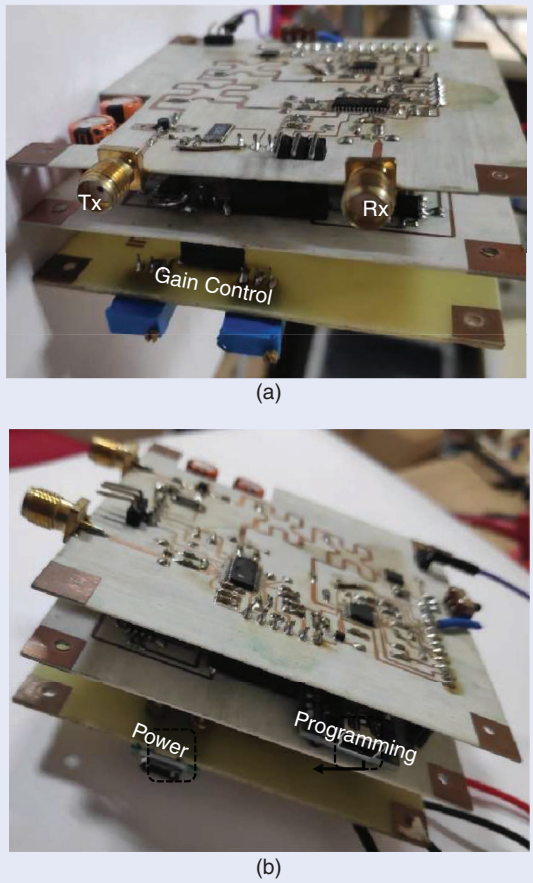

Figure 15. *(a) and (b) A 3D view of the integrated radar module, highlighting its various external pin connections.*

The following equation provides the stable transmitted radar signal, illustrating the relationship between the output VCO frequency, the control bits, and the counters, as depicted in the PLL-VCO block diagram in (9):

$$f_{\mathrm{VCO}} = \frac{[(P \times B) + A] \times f_{\mathrm{REFIN}}}{R}. \tag{17}$$

where f_{VCO} is the frequency obtained from the VCO, P is the preset modulus of the prescaler, A is the preset divide ratio of the 5-bit N counter, B is the preset divide ratio of the 13-bit N counter, f_{REFIN} is the reference frequency, and R is preset divide ratio of the R counter.

According to the datasheet, the "MSBFIRST" bit order is used for data transfer, and "SPI MODE0" is selected for synchronization. The ADI PLL N-int software is employed to generate the hexadecimal codes necessary to produce the desired frequency. A snapshot of the open source software used is shown in Figure 13. For a detailed description, readers can refer to the ADF4118 PLL datasheet [58].

The analog pin A3 of the Arduino is used to read and display voltage information. It's important to note that the hexadecimal codes for a single frequency can vary depending on the reference frequency and mode of operation. The software used for generating the hex codes accounts for these variations. In the radar

module design, a reference frequency of 10 MHz is used. The steps to generate an RF frequency of 2.5 GHz are summarized in Figure 14.

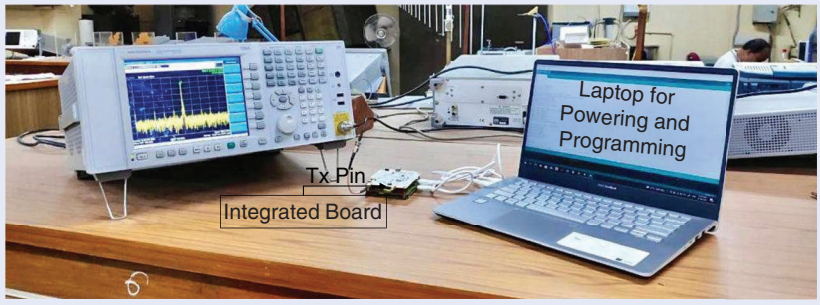

Figure 16. *Testing of the integrated module, with the Tx pin connected to the spectrum analyzer, and the power and microcontroller pins connected directly to the laptop.*

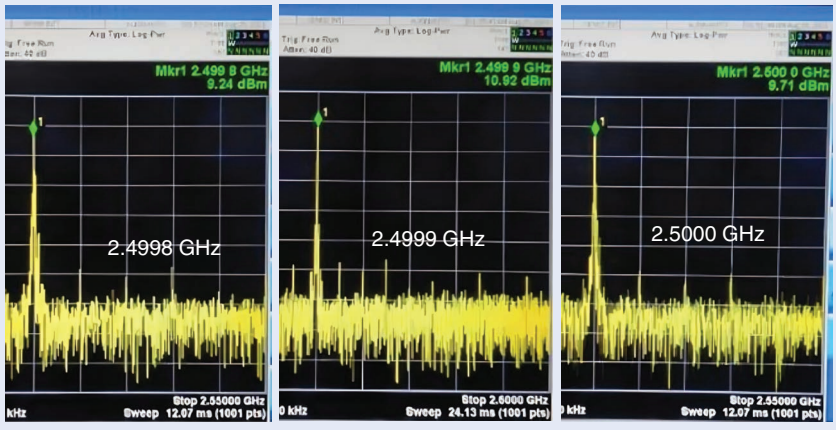

Figure 17. *(a)–(c) A spectrum analyzer display of Tx spectrum at (a) 2.4998 GHz, (b) 2.4999 GHz, and (c) 2.5000 GHz.*

In this work, I/Q data were collected using the analog pins of an Arduino Nano and stored in a data file for further analysis. This data collection facilitates the extraction of Doppler signals for human motion detection or other applications.

The Arduino Nano's ADC operates with a 10-bit resolution and a maximum sampling rate of 10 kHz [59]. This 10-bit resolution provides a sufficiently detailed representation of the I/Q data, critical for accurate signal processing. To enhance the analysis and visualization capabilities, additional test points are integrated into the design, allowing results to be directly observed on a digital oscilloscope (DSO).

Validation and Testing

The 3D model of the radar module is illustrated in Figure 15, showcasing its design and configuration. The module is powered via a laptop, as depicted in the image, while the Tx pin is directly connected to a spectrum analyzer, as shown in Figure 16.

To verify the frequency controllability of the radar module, an experiment was conducted where the RF frequency was initially set to

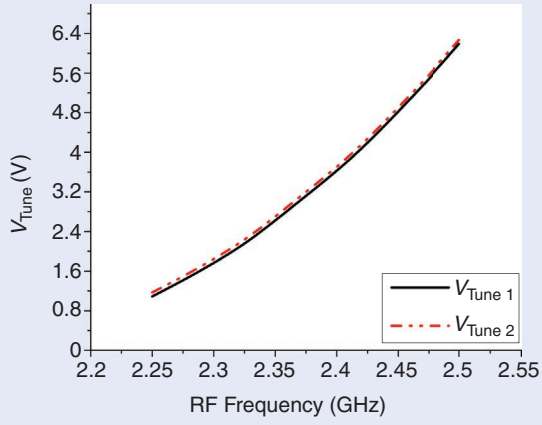

Figure 18. *The VCO voltage tuning curve at two different time stamps.*

Figure 19. *The I/Q time-domain signal of the vibrating object on a DSO.*

2.4998 GHz. The frequency was then systematically increased in 100-kHz intervals across three consecutive RF frequencies. The results of this frequency adjustment are illustrated in Figure 17, demonstrating the radar's ability to operate across a range of frequencies and maintain precise control.

Subsequently, the tuning voltage readings V_{tune1} of the VCO were examined by incrementally increasing the RF frequencies in 25-MHz steps over the range of 2.25–2.5 GHz. The voltage corresponding to each frequency was recorded and displayed on the computer's serial monitor. The radar module was then operated continuously throughout the day, and similar tuning voltage readings V_{tune2} were captured at the end of the day to assess the long-term stability.

The results, plotted in Figure 18, reveal a slight deviation of 80 mV in the tuning voltage range. However, the data also indicate that the VCO-PLL loop effectively maintained RF frequency stability over the duration of the test. This demonstrates that the radar module exhibits reliable frequency control and stability, validating its performance for consistent operation in practical applications.

Following the RF testing, the radar module was evaluated for I/Q performance. The significance of I/Q for identifying null and optimum points was verified using a motor and metal plate to simulate a constant vibration source. The Tx RF frequency was set to 2.4 GHz via the SPI command, and to ensure precise validation, the vibrating object was positioned approximately 3 m from the radar. Both I and Q outputs were connected to a DSO, as depicted in Figure 19.

Subsequently, the detection of human activities was also tested. The transmitted frequency was fixed at 2.4 GHz, and a person was positioned about 5 m from the radar, performing two types of movements: standing still and spot-running toward the radar. The experimental setup is shown in Figure 20, with the time-domain I-phase data displayed on the DSO in Figure 21. I-phase data was recorded for 60 s for both conditions, and short-time Fourier transform (STFT) analysis was conducted in MATLAB. The results for the two different conditions are presented in Figure 22,

Figure 20. *Photographs of the experimental setup for human activity determination.*

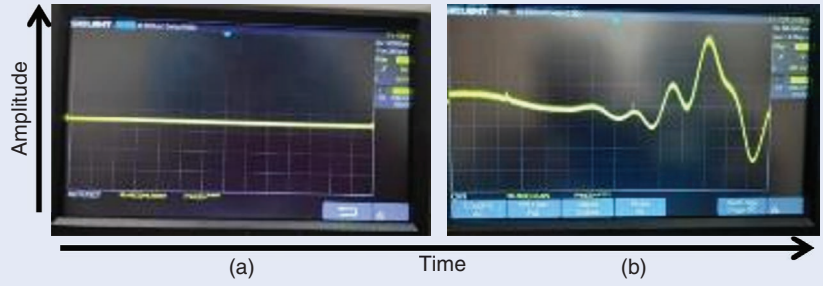

Figure 21. *(a) and (b) The time-domain baseband signal of the I-phase component for a person standing still and for one performing spot jogging.*

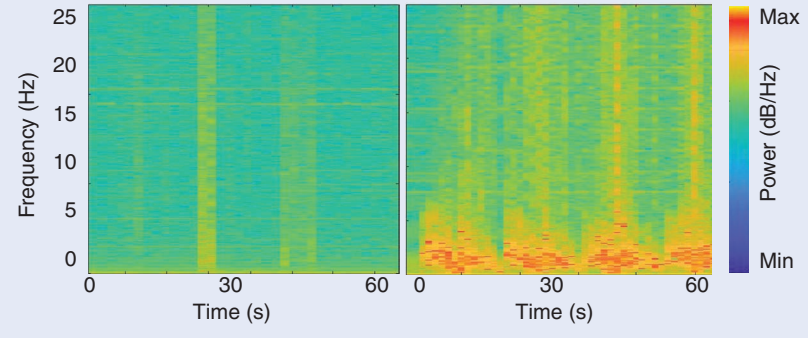

Figure 22. *The STFT of the I-phase signal for a person standing still and for one performing spot jogging.*

demonstrating the radar's capability to detect and differentiate between various human activities.

Based on the results obtained, it is clear that the designed radar system effectively analyzes human movement, providing a distinct signature that is invaluable for security applications. Additionally, the radar's capability to monitor vibrating sources using both I and Q signals expands its utility for various experimental purposes, including vibration monitoring and generating datasets for machine learning and AI applications. Enhanced signal processing allows for the extraction of phase information, offering detailed insights into the dynamics of both approaching and departing targets.

This performance underscores the substantial potential of the portable radar design for students and researchers, offering significant value for diverse research and educational applications. The successful validation of the design methodology demonstrates the radar module's effectiveness and reliability in practical and academic contexts, confirming its contribution to advancing understanding of radar technology and its varied applications.

Conclusion

In this article, we have thoroughly explored the design and implementation of a portable radar module, from fundamental radar principles to detailed architecture. The module's integration of I/Q components significantly enhances the detection reliability by eliminating null points, demonstrating its robustness for various applications. Experimental validation has confirmed the design's effectiveness, showcasing the radar module's practical utility and its educational value by providing hands-on experience with radar technology. This comprehensive approach not only advances our understanding of radar systems but also supports educational initiatives by enabling practical experimentation and learning.

Acknowledgment

The authors would like to acknowledge the IEEE MTT-S Pre-Graduate Scholarship-2021 for the motivation and partial funding of this research [60]. Special thanks to Jagannath Mukhi for his contribution to the in-house fabrication process. The authors also extend their gratitude to Ayan Sharma for his invaluable assistance in building the LaTeX file for this article and Bishal Kashyap for his help in designing the illustrations for this article.

References

[1] T. K. Sarkar, M. Salazar Palma, and E. L. Mokole, "Echoing across the years: A history of early radar evolution," *IEEE Microw. Mag.*, vol. 17, no. 10, pp. 46–60, Oct. 2016, doi: 10.1109/MMM.2016.2589200.

[2] Y. Kalkan, "Frequency-only radars and other frequency-based systems with applications," *IEEE Microw. Mag.*, vol. 17, no. 7, pp. 26–52, Jul. 2016, doi: 10.1109/MMM.2016.2541821.

[3] C. Li et al., "A review on recent progress of portable short-range noncontact microwave radar systems," *IEEE Trans. Microw. Theory Techn.*, vol. 65, no. 5, pp. 1692–1706, May 2017, doi: 10.1109/TMTT.2017.2650911.

[4] M. Kebe et al., "Human vital signs detection methods and potential using radars: A review," *Sensors*, vol. 20, no. 5, 2020, Art. no. 1454, doi: 10.3390/s20051454.

[5] C. Li, V. M. Lubecke, O. Boric-Lubecke, and J. Lin, "A review on recent advances in Doppler radar sensors for noncontact healthcare monitoring," *IEEE Trans. Microw. Theory Techn.*, vol. 61, no. 5, pp. 2046–2060, May 2013, doi: 10.1109/TMTT.2013.2256924.

[6] J.-M. Muñoz-Ferreras, Z. Peng, R. Gómez-García, and C. Li, "Review on advanced short-range multimode continuous-wave radar architectures for healthcare applications," *IEEE J. Electromagn., RF, Microw. Med. Biol.*, vol. 1, no. 1, pp. 14–25, Jun. 2017, doi: 10.1109/JERM.2017.2735241.

[7] S. Dong et al., "A review on recent advancements of biomedical radar for clinical applications," *IEEE Open J. Eng. Med. Biol.*, vol. 5, pp. 1–18, 2024, doi: 10.1109/OJEMB.2024.3401105.

[8] S. A. Shah and F. Fioranelli, "RF sensing technologies for assisted daily living in healthcare: A comprehensive review," *IEEE Aerosp. Electron. Syst. Mag.*, vol. 34, no. 11, pp. 26–44, Nov. 2019, doi: 10.1109/MAES.2019.2933971.

[9] J. Lin, "Noninvasive microwave measurement of respiration," *Proc. IEEE*, vol. 63, no. 10, pp. 1530–1530, Oct. 1975, doi: 10.1109/PROC.1975.9992.

[10] F. Quaiyum, and others., "Noncontact human gait analysis and limb joint tracking using Doppler radar," *IEEE J. Electromagn., RF, Microw. Med. Biol.*, vol. 3, no. 1, pp. 61–70, Mar. 2019, doi: 10.1109/JERM.2018.2881238.

[11] Y. Kim, S. Ha, and J. Kwon, "Human detection using Doppler radar based on physical characteristics of targets," *IEEE Geosci. Remote Sens. Lett.*, vol. 12, no. 2, pp. 289–293, Feb. 2015, doi: 10.1109/LGRS.2014.2336231.

[12] S. Ahmed and S. H. Cho, "Machine learning for healthcare radars: Recent progresses in human vital sign measurement and activity recognition," *IEEE Commun. Surveys Tuts.*, vol. 26, no. 1, pp. 461–495, 1st Quart. 2024, doi: 10.1109/COMST.2023.3334269.

[13] I.-S. Lee and J.-R. Yang, "Signal preprocessing for heartbeat detection using continuous-wave Doppler radar," *IEEE Microw. Wireless Compon. Lett.*, vol. 33, no. 4, pp. 479–482, Apr. 2023, doi: 10.1109/LMWT.2022.3228328.

[14] Y. Li, Z. Peng, R. Pal, and C. Li, "Potential active shooter detection based on radar micro-Doppler and range-Doppler analysis using artificial neural network," *IEEE Sensors J*, vol. 19, no. 3, pp. 1052–1063, Feb. 2019, doi: 10.1109/JSEN.2018.2879223.

[15] V. Lubecke, O. Borić-Lubecke, M. S. Ishrak, T. Wu, and F. Cai, "Radar monitoring in sleep medicine," in *Proc. 16th Int. Conf. Adv. Technol., Syst. Services Telecommun. (TELSIKS)*, 2023, pp. 109–113, doi: 10.1109/TELSIKS57806.2023.10316075.

[16] Z. Xia, M. M. H. Shandhi, O. T. Inan, and Y. Zhang, "Non-contact sensing of seismocardiogram signals using microwave Doppler radar," *IEEE Sensors J.*, vol. 18, no. 14, pp. 5956–5964, Jul. 2018, doi: 10.1109/JSEN.2018.2842122.

[17] M. Nouman, S. Y. Khoo, M. A. P. Mahmud, and A. Z. Kouzani, "Recent advances in contactless sensing technologies for mental health monitoring," *IEEE Internet Things J.*, vol. 9, no. 1, pp. 274–297, Jan. 2022, doi: 10.1109/JIOT.2021.3097801.

[18] V. G. Rizzi Varela and C. Li, "Wind turbines structural health monitoring using a FMCW radar mounted on a drone," in *Proc. IEEE Topical Conf. Wireless Sensors Sensor Netw. (WiSNeT)*, 2024, pp. 15–17, doi: 10.1109/WiSNeT59910.2024.10438590.

[19] P. K. Gogoi, M. K. Mandal, A. Kumar, and T. Chakravarty, "A 2.4 GHz compact Doppler radar module for vibration monitoring," in *Proc. IEEE MTT-S Int. Microw. RF Conf. (IMARC)*, 2019, pp. 1–4, doi: 10.1109/IMaRC45935.2019.9118746.

[20] A. Bhattacharya. "Principles and techniques of modern radar systems." NPTEL. Accessed: Jan. 12, 2024. [Online]. Available: https://onlinecourses.nptel.ac.in/noc19_ee58/preview

[21] R. M. O. Donnell. "Radar introduction to radar systems — Online course." MIT Lincoln Laboratory. [Online]. Available: https://www.ll.mit.edu/outreach/radar-introduction-radar-systems-online-course

[22] D. Schor and T. Kakarountas, "The benefits of engineering design competitions," *IEEE Potentials*, vol. 40, no. 4, pp. 4–5, Jul./Aug. 2021, doi: 10.1109/MPOT.2021.3073727.

[23] S. Mann, F. Lurz, R. Weigel, and A. Koelpin, "A high-sensitivity radar system featuring low weight and power consumption," *IEEE Microw. Mag.*, vol. 16, no. 2, pp. 99–105, Mar. 2015, doi: 10.1109/MMM.2014.2367860.

[24] T. Jaeschke, C. Bredendiek, S. Küppers, and N. Pohl, "High-precision D-band FMCW-radar sensor based on a wideband SiGe-transceiver MMIC," *IEEE Trans. Microw. Theory Techn.*, vol. 62, no. 12, pp. 3582–3597, Dec. 2014, doi: 10.1109/TMTT.2014.2365460.

[25] D. Rodriguez, D. V. Q. Rodrigues, A. Mishra, M. A. Saed, and C. Li, "Quadrature and single-channel low-cost monostatic radar based on a novel 2-port transceiver chain," *IEEE Sensors J.*, vol. 23, no. 23, pp. 28,872–28,882, Dec. 2023, doi: 10.1109/JSEN.2023.3324882.

[26] M. Dwyer and D. S. Ricketts, "The North Carolina state university rabbit radar: Build a frequency-modulated continuous-wave radar in a day [Application Notes]," *IEEE Microw. Mag.*, vol. 21, no. 5, pp. 136–145, May 2020, doi: 10.1109/MMM.2020.2971184.

[27] B. Schweizer et al., "The fairy tale of simple all-digital radars: How to deal with 100 gbit/s of a digital millimeter-wave MIMO radar on an FPGA [Application Notes]," *IEEE Microw. Mag.*, vol. 22, no. 7, pp. 66–76, Jul. 2021, doi: 10.1109/MMM.2021.3069602.

[28] G. L. Charvat, A. J. Fenn, and B. T. Perry, "The MIT IAP radar course: Build a small radar system capable of sensing range, Doppler, and synthetic aperture (SAR) imaging," in *Proc. IEEE Radar Conf.*, 2012, pp. 0138–0144, doi: 10.1109/RADAR.2012.6212126.

[29] P. K. Gogoi, "It's all about connections [MiT society news]," *IEEE Microw. Mag.*, vol. 22, no. 6, pp. 100–103, 2021, doi: 10.1109/MMM.2021.3064777.

[30] J. Larson, S. S. Jordan, M. Lande, and S. Weiner, "Supporting self-directed learning in a project-based embedded systems design course," *IEEE Trans. Educ.*, vol. 63, no. 2, pp. 88–97, <doi: 10.1109/TE.2020.2975358.

[31] E. Kim and G. J. Strimel, "The influence of entrepreneurial mindsets on student design problem framing," *IEEE Trans. Educ.*, vol. 63, no. 2, pp. 126–135, May 2020, doi: 10.1109/TE.2019.2918253.

[32] E. W. Engstrom, "Systems engineering: A growing concept," *Elect. Eng.*, vol. 76, no. 2, pp. 113–116, Feb. 1957, doi: 10.1109/EE.1957.6442968.

[33] P. K. Gogoi, M. K. Mandal, A. Kumar, and T. Chakravarty, "A compact multi-mode integrated Doppler radar at 2.4 ghz for multipurpose applications," in *Proc. IEEE Wireless Antenna Microw. Symp. (WAMS)*, 2022, pp. 1–4, doi: 10.1109/WAMS54719.2022.9848033.

[34] M. I. Skolnik, *Radar Handbook*, 3rd ed. New York, NY, USA: McGraw-Hill, 2008.

[35] V. C. Chen, D. Tahmoush, and W. J. Miceli, Eds., *Radar Micro-Doppler Signatures: Processing and Applications*. London, U.K.: Inst. Eng. Technol., 2014.

[36] A. Droitcour, O. Boric-Lubecke, V. Lubecke, J. Lin, and G. Kovacs, "Range correlation and I/Q performance benefits in single-chip silicon Doppler radars for noncontact cardiopulmonary monitoring," *IEEE Trans. Microw. Theory Techn.*, vol. 52, no. 3, pp. 838–848, Mar. 2004, doi: 10.1109/TMTT.2004.823552.

[37] M. Budge and M. Burt, "Range correlation effects on phase and amplitude noise," in *Proc. Southeastcon*, Charlotte, NC, USA, 1993, p. 5.

[38] B.-K. Park, S. Yamada, O. Boric-Lubecke, and V. Lubecke, "Single-channel receiver limitations in Doppler radar measurements of periodic motion," in *Proc. IEEE Radio Wireless Symp.*, 2006, pp. 99–102, doi: 10.1109/RWS.2006.1615104.

[39] J. Wang, X. Wang, L. Chen, J. Huangfu, C. Li, and L. Ran, "Non-contact distance and amplitude-independent vibration measurement based on an extended DACM algorithm," *IEEE Trans. Instrum. Meas.*, vol. 63, no. 1, pp. 145–153, Jan. 2014, doi: 10.1109/TIM.2013.2277530.

[40] C. Li and J. Lin, "Complex signal demodulation and random body movement cancellation techniques for non-contact vital sign detection," in *Proc. IEEE MTT-S Int. Microw. Symp. Dig.*, 2008, pp. 567–570, doi: 10.1109/MWSYM.2008.4633229.

[41] B.-K. Park, O. Boric-Lubecke, and V. M. Lubecke, "Arctangent demodulation with DC offset compensation in quadrature Doppler radar receiver systems," *IEEE Trans. Microw. Theory Techn.*, vol. 55, no. 5, pp. 1073–1079, May 2007, doi: 10.1109/TMTT.2007.895653.

[42] R. Svitek and S. Raman, "DC offsets in direct-conversion receivers: Characterization and implications," *IEEE Microw. Mag.*, vol. 6, no. 3, pp. 76–86, Sep. 2005, doi: 10.1109/MMW.2005.1511916.

[43] R. Moraes and D. Evans, "Compensation for phase and amplitude imbalance in quadrature Doppler signals," *Ultrasound Med. Biol.*, vol. 22, no. 1, pp. 129–137, 1996, doi: 10.1016/0301-5629(95)02027-6.

[44] "HMC385 datasheet," 2024. Accessed: Aug. 9, 2009. [Online]. Available: https://www.analog.com/media/en/technical-documentation/data-sheets/hmc385.pdf

[45] "ADF4118 datasheet," 2024. [Online]. Available: https://www.analog.com/media/en/technical-documentation/data-sheets/ADF4116_4117_4118.pdf

[46] "DSC6003HI3B datasheet," 2024. [Online]. Available: https://nl.mouser.com/datasheet/2/268/DSC60xxB_Ultra_Small_Ultra_Low_Power_MEMS_Oscillat-3075561.pdf

[47] "AD8347 datasheet," 2024. [Online]. Available: https://www.analog.com/media/en/technical-documentation/data-sheets/AD8347.pdf

[48] T. Qi, S. He, Z. Dai, and W. Shi, "Novel unequal dividing power divider with 50-ohm characteristic impedance lines," *IEEE Microw. Wireless Compon. Lett.*, vol. 26, no. 3, pp. 180–182, Mar. 2016, doi: 10.1109/LMWC.2016.2525817.

[49] "AG302 datasheet," 2024. [Online]. Available: https://www.qorvo.com/products/p/AG302-86G

[50] "HHM17146A1 datasheet," 2024. [Online]. Available: https://product.tdk.com/system/files/dam/doc/product/rf/rf/balun/catalog/rf_balun_hhm17146a1_en.pdf

[51] "Designing high-performance phase-locked loops with high-voltage," 2024. [Online]. Available: https://www.analog.com/en/resources/analog-dialogue/articles/designing-plls-with-high-voltage-vcos.html

[52] "ADIsimPLL," 2024. [Online]. Available: https://www.analog.com/en/lp/resources/adisimpll.html

[53] "LM385B datasheet," 2024. [Online]. Available: https://shorturl.at/Mw4UT

[54] A. B. Carman and C. Li, "Passive multistatic wireless sensing based on discrete LNA/mixer co-optimization and fast-startup baseband amplifier," in *Proc. IEEE Topical Conf. Wireless Sensors Sensor Netw.*, 2023, pp. 43–45 doi: 10.1109/WiSNeT56959.2023.10046263.

[55] "LP5912 datasheet," 2024. [Online]. Available: https://shorturl.at/MEzsG

[56] "MAX1683 datasheet," 2024. [Online]. Available: https://www.analog.com/media/en/technical-documentation/data-sheets/max1682-max1683.pdf

[57] "LM27762 datasheet," 2024. [Online]. Available: https://www.ti.com/lit/ds/symlink/lm27762.pdf?ts=1723221887897&ref_url=https\%253A\%252F\%252Fwww.google.com\%252F

[58] "ADIsimPLLSoftware." URL Shortener. Accessed: Jan. 12, 2024. [Online]. Available: https://shorturl.at/o8y0N

[59] "Arduino nano," 2024. [Online]. Available: https://store.arduino.cc/products/arduino-nano

[60] Z. Marinković, P. J. Soh, R. Henderson, R. Mansour, and W. C. Cherry, "The 2020 and 2021 MTT-S undergraduate/pre-graduate scholarship awards [Education News]," *IEEE Microw. Mag.*, vol. 23, no. 8, pp. 34–109, Aug. 2022, doi: 10.1109/MMM.2022.3173071.